Catalysis Science & Technology

ROYAL SOCIETY OF CHEMISTRY

PAPER

View Article Online
View Journal | View Issue

Cite this: *Catal. Sci. Technol.*, 2022, **12**, 664

Heterogenisation of a carbonylation catalyst on dispersible microporous polymer nanoparticles†

Samuel A. Ivko, ‡[a] Alex M. James, §[a] Matthew J. Derry, [b] Robert Dawson *[a] and Anthony Haynes *[a]

Received 2nd November 2021,
Accepted 11th December 2021

DOI: 10.1039/d1cy01989a

rsc.li/catalysis

The methanol carbonylation catalyst, *cis*-$[Rh(CO)_2I_2]^-$, has been heterogenised within a dispersible microporous polymer support bearing cationic functionality. The microporous polymer has a core–shell structure in which the porous and insoluble core (a cross-linked co-polymer of divinylbenzene and 4-vinylpyridine) is sterically stabilised by long hydrophilic poly(ethylene glycol) chains, allowing a stable nanoparticle dispersion to form. Incorporation of 4-vinylpyridine as a co-monomer allows post-synthetic modification to generate *N*-methylpyridinium sites for electrostatic attachment of the anionic rhodium(I) complex. The dispersibility of the polymer-supported catalyst material facilitates the use of *in situ* transmission IR spectroscopy to obtain kinetic data for the oxidative addition of iodomethane to immobilised *cis*-$[Rh(CO)_2I_2]^-$ (the rate-limiting step of the carbonylation cycle). The kinetic data followed a double exponential decay, with an initial fast phase having a rate constant k_2^1 that is ~5× greater than k_2^2 for the slow phase (where k_2^2 is similar to the homogeneous system using *N*-methylpyridinium counter-ions, CH_2Cl_2, 25 °C). The polymer-supported catalyst was found to be active for carbonylation of MeOH/MeI to give methyl acetate, with an initial rate *ca.* double that of the homogeneous analogue under the same conditions (10 bar CO, MeI/MeOH, 120 °C). Activity is lost over longer periods due to leaching of Rh from the support.

Introduction

Homogeneous transition metal catalysts are widely used for organic transformations on laboratory and bulk scales.[1] They typically benefit from high activity and selectivity under relatively mild conditions, and can be tuned by choice of metal, ligand, solvent and reaction conditions. Compared with heterogeneous catalysts, however, they suffer from the need to separate product from a solution phase containing the dissolved catalyst. Typically, a distillation is required under conditions that can lead to catalyst degradation and incur significant costs.[2] In order to combine the benefits of both homogeneous and heterogeneous catalysis, a common approach is to immobilise a soluble metal complex on an insoluble support such as an inorganic oxide, zeolite, metal–organic framework or organic polymer.[3]

One of the most significant commercial bulk processes that uses homogeneous transition metal catalysis is the carbonylation of methanol to produce acetic acid (global demand ~20 million tonnes p.a.[4]), employing rhodium- or iridium-based catalysts.[5–9] The Monsanto process, developed in the 1960s, employs a rhodium catalyst and an iodide promoter, achieving very high selectivity (>99% based on MeOH).[10] The active rhodium complex is a square-planar Rh(I) species, *cis*-$[Rh(CO)_2I_2]^-$, which undergoes oxidative addition of methyl iodide, derived from the methanol feedstock (Scheme 1).

To maintain high activity and catalyst stability, as well as to improve solubility, a relatively high concentration of water (~10% wt) is used in the reaction medium. At lower water concentrations, an inactive Rh(III) species, $[Rh(CO)_2I_4]^-$, can accumulate as an intermediate in a competing water gas shift (WGS) reaction.[11] This species can dissociate CO and lead to precipitation of RhI_3 in parts of the plant that have lower CO partial pressure. Although high water concentration alleviates this, it increases the cost of product purification, by distillation, to produce dry acetic acid. Variations of the Monsanto process have been introduced that allow operation at lower water concentration. For example, the Celanese Acid Optimisation (AO Plus) technology employs lithium iodide as

[a] *Department of Chemistry, University of Sheffield, Sheffield, S3 7HF, UK. E-mail: a.haynes@sheffield.ac.uk*
[b] *Aston Institute of Materials Research, Aston University, Birmingham, B4 7ET, UK*

† Electronic supplementary information (ESI) available: Details of materials and synthetic methods, instrumentation, analytical, gas sorption, dispersibility and kinetic data, determination of TOF values (PDF). See DOI: 10.1039/d1cy01989a

‡ Current address: School of Chemistry, University of Birmingham, Birmingham, B15 2TT, UK.
§ Current address: Materials Innovation Factory, University of Liverpool, Liverpool, L7 3NY, UK.

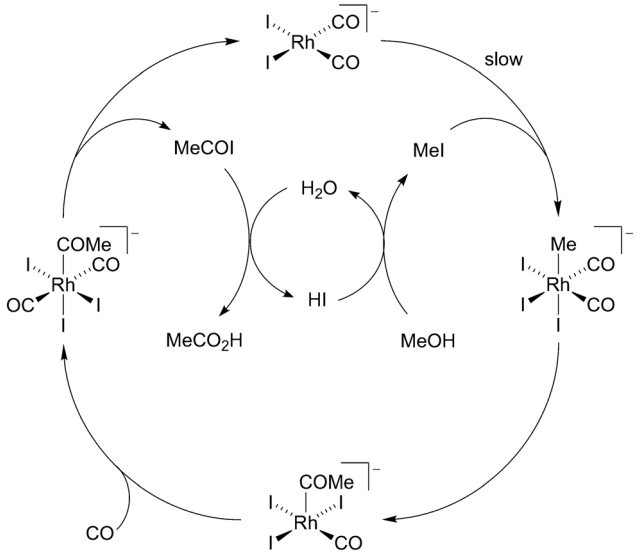

Scheme 1 Cycle for rhodium/iodide catalysed methanol carbonylation.

an additive that stabilises the Rh catalyst and maintains high carbonylation activity at significantly lower water concentration.[12–14] Related Rh-catalysed processes for carbonylation of methyl acetate to acetic anhydride under anhydrous conditions use lithium iodide or acetate (Eastman)[15] or quaternary ammonium iodide salts (BP Chemicals).[16] BP Chemicals' Cativa™ process uses a promoted iridium/iodide homogeneous catalyst system that achieves high activity and selectivity for methanol carbonylation at low water concentration.[17,18]

Another approach to minimise problems with solubility at low water concentration is to heterogenise the catalyst by immobilisation on a solid support.[5,16,19] A range of support materials that bind the Rh catalyst directly through a covalent interaction have been investigated, including inorganic oxides,[20,21] zeolites,[22–25] polymers,[26–31] carbon[32] and covalent triazine frameworks.[33] Many of these systems exhibit reaction rates slower than that of the homogeneous process, likely due, in part, to the covalent tethering of the catalyst, which modifies the first coordination sphere of the Rh complex. Leaching of catalyst due to lability of the Rh–support interaction can also be problematic.

An alternative strategy for heterogenisation, which preserves the first coordination sphere of the catalyst, is immobilisation of the anionic Rh complex on a cationic support by electrostatic interactions.[34–37] This approach has been observed to result in less catalyst leaching compared with covalent tethering. In 1981, Drago *et al.* described the effective immobilisation of *cis*-$[Rh(CO)_2I_2]^-$ on polymer supports based on *N*-methylated polyvinylpyridines.[38] The carbonylation activity was equal to the homogeneous system at 120 °C with minimal leaching of the supported catalyst. This ionic attachment approach was adopted in the Acetica™ process developed by Chiyoda and UOP which employs a polyvinylpyridine resin tolerant of catalytic reaction conditions and a bubble column loop reactor that minimises catalyst attrition compared to conventional stirring.[39] The pyridyl groups are quaternised in the presence of iodomethane, and the anionic catalyst, *cis*-$[Rh(CO)_2I_2]^-$ is bound electrostatically to the support. The supported catalyst showed no deactivation after continuous operation for 7000 hours and its activity is competitive with the homogeneous process, with decreased by-product formation *via* the WGS reaction due to the lower water concentration employed.

The catalytic mechanism for this type of supported system was investigated by Haynes *et al.* using cross-linked poly(4-vinylpyridine-*co*-styrene-*co*-divinylbenzene) in the form of thin films suitable for *in situ* transmission IR spectroscopy.[40] *N*-Methylation with methyl iodide and subsequent reaction with $[Rh(CO)_2I]_2$ generated the electrostatically bound complex *cis*-$[Rh(CO)_2I_2]^-$ (Scheme 2). EXAFS measurements indicated that the structure of supported *cis*-$[Rh(CO)_2I_2]^-$ is essentially the same as determined crystallographically for the *N*-methylpyridinium salt and IR spectroscopic monitoring showed that the same organometallic steps occur for the supported complex as in solution, with kinetics of MeI oxidative addition comparable to the solution phase.

Microporous polymers have also been widely investigated for heterogeneous catalysis,[41–43] including their use to encapsulate metal catalysts electrostatically.[44–46] Recently, a new class of dispersible porous polymer has been reported, synthesised using reversible addition–fragmentation chain transfer-mediated polymerisation-induced self-assembly (RAFT-mediated PISA).[47] Co-polymerisation of divinylbenzene (DVB) and fumaronitrile (FN) was mediated using a hydrophilic macromolecular chain transfer agent (macro-CTA) in an anti-solvent for the growing polymer chain. This resulted in the formation of polymer nanoparticles with a core–shell morphology. The high degree of cross-linking within the core of the sample means that the material is microporous in nature. However, unlike most other porous polymers, these materials can form stable dispersions in a variety of organic solvents for long periods of time, permitting them to be processed and utilised for applications in the solution phase. Furthermore, their recovery from solution can be achieved either *via* addition of an anti-solvent or centrifugation. The combination of inexpensive

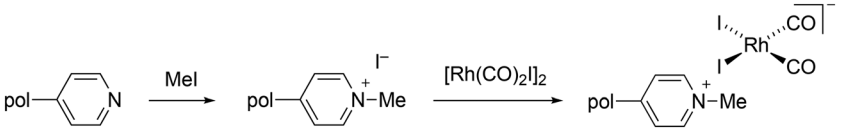

Scheme 2 Route to ionically attached *cis*-$[Rh(CO)_2I_2]^-$.

synthesis, high surface area, microporosity, robust chemical stability and dispersibility makes them ideal candidates for catalyst immobilisation. Ferguson *et al.* recently utilised this approach to synthesise dispersible porous polymer photocatalytic nanoparticles, which were found to be active for a range of photocatalytic reactions to produce pharmaceutically relevant compounds.[48] The versatility of these porous materials for encapsulation of molecular species has also recently been demonstrated in the formation of organic white-light emitting dispersions.[49]

Here we report the synthesis of a new dispersible porous material by co-polymerisation of 4-vinylpyridine (4VP) with DVB in the presence of a PEG-based macro-CTA. The 4VP functionality allows the material to be post-synthetically modified using iodomethane to generate a cationic support which is used to bind *cis*-$[Rh(CO)_2I_2]^-$ electrostatically. The organometallic steps of the methanol carbonylation cycle can be followed by *in situ* IR spectroscopy for the supported catalyst and rate measurements show more complex kinetic behaviour for the oxidative addition of MeI to *cis*-$[Rh(CO)_2I_2]^-$ than in homogeneous solution. Catalytic formation of methyl acetate from MeOH/MeI under relatively mild conditions is demonstrated, although a loss of catalytic activity with time occurs, which is attributed to leaching of Rh catalyst. Despite this, our results indicate that this class of material has considerable potential for the development of supported catalysts that operate under less forcing conditions.

Results and discussion

Synthesis and characterisation of supported catalyst

Synthesis of the dispersible porous polymeric material **1** employed a RAFT-mediated PISA approach analogous to that reported by James *et al.*[47] whereby DVB and 4VP monomers were co-polymerised in a 1 : 1 (w/w) ethanol : water solvent mixture using a PEG-based macro-CTA (Scheme 3). Post-synthetic modification (PSM) of **1** was accomplished by treatment with MeI to give the *N*-methylated polymer, **2**, followed by addition of the rhodium dimer, $[Rh(CO)_2I]_2$, to generate the supported catalyst material **3**.

Materials **1–3** were characterised using IR and solid-state NMR spectroscopy, together with elemental and ICP-MS analysis. The cross-linked structures means that the materials are insoluble, and not amenable to GPC analysis. Product **1** was obtained as a white solid after extraction of unreacted monomer and drying *in vacuo*. The nitrogen content of **1** indicates incomplete incorporation of the 4VP monomer and an approximate average composition of the polymer is estimated to be $PEG_{113}DVB_{300}4VP_{60}$. After reaction with iodomethane, giving **2** as a yellow powder, the iodide content is consistent with approximately 80% of the 4VP units having been *N*-methylated (Table S1†).

The IR spectra of all three materials (Fig. 1(a)) show bands at 994 cm^{-1} assigned to ν(C–O) of the ether linkages of the solubilising PEG chains. Absorptions at 3030 and 1195 cm^{-1} are characteristic of aromatic ν(C–H) and ν(C–N) modes of the DVB and 4VP units respectively and bands centred at 2930 and 1450 cm^{-1} represent the aliphatic C–H stretching and bending modes respectively. The solid state $^{13}C\{^1H\}$ CP/MAS NMR spectra of **1–3** (Fig. 1(b)) each show a broad resonance at δ 40 ppm corresponding to the aliphatic carbons of the polymer backbone. This broad signal presumably obscures the expected peak due to the *N*-methyl groups of quaternised 4VP units in **2** and **3** (reported to occur at δ 49.8 ppm for *N*-methylpyridinium iodide in ethanol solution[50]). All the materials also show a small resonance at δ 70 ppm due to the solubilising PEG chains, consistent with polymerisation being mediated through the RAFT macro-CTA. Peaks between δ 120 and 160 ppm correspond to the aromatic carbons of the two monomer units for material **1**.

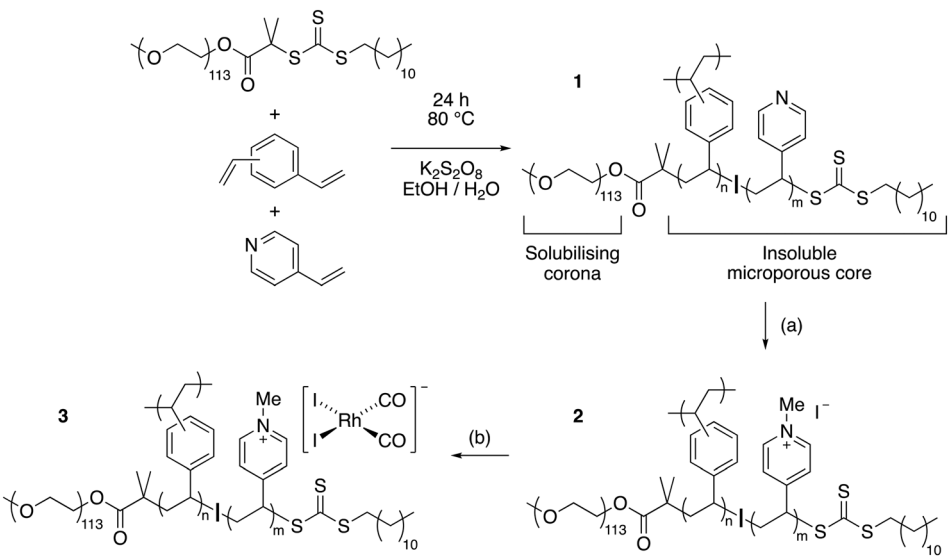

Scheme 3 Synthesis of pyridine-containing dispersible microporous polymer (**1**), post-synthetic *N*-methylation to form **2** and subsequent reaction with $[Rh(CO)_2I]_2$ to form **3**; (a) MeI in $CHCl_3$, 70 °C, 72 h; (b) $[Rh(CO)_2I]_2$ in $CHCl_3$, RT, 16 h.

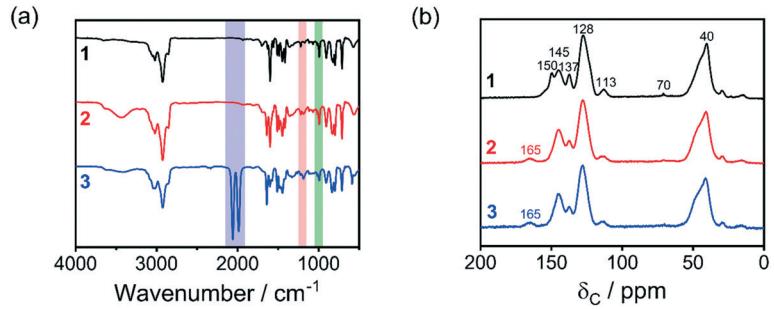

Fig. 1 (a) FTIR spectra highlighting the absorptions due to ν(C–N) (green), ν(C–O) (red) and ν(C≡O) (blue); (b) solid state $^{13}C\{^1H\}$ CP/MAS NMR of materials **1** (black), **2** (red) and **3** (blue).

The resonance centred at δ 150 ppm is lost in **2** and **3**, accompanied by the appearance of a new signal at δ 165 ppm, assigned to the *para* carbon of the pyridine moiety, by analogy to the downfield shift that occurs in solution on *N*-methylation of pyridine.[50] A resonance at δ 113 ppm, in the spectra of all three materials, is attributed to the presence of some unreacted vinyl moieties of the DVB monomer units.

On addition of a chloroform solution of $[Rh(CO)_2I]_2$ to **2**, uptake of Rh complex by the polymer was indicated by the supernatant phase becoming colourless. Removal of solvent gave **3** as a brown powder and ICP-MS analysis showed **3** to contain 4.5% Rh by weight. The IR spectrum of **3** shows two strong ν(CO) absorptions at 2062 and 1990 cm^{-1} which are very close to those reported for the anionic rhodium complex, *cis*-$[Rh(CO)_2I_2]^-$, in solution.[51,52] In a control experiment, reaction of the non-quaternised material **1** with $[Rh(CO)_2I]_2$ gave a product with ν(CO) bands at 2080 and 2010 cm^{-1}, the higher frequencies being consistent with coordination of a pyridyl moiety in **1** to form a covalently attached neutral complex $[Rh(CO)_2I$(py-**1**)$]$.

To assess the porosity and surface area of **1**–**3**, volumetric gas sorption studies using nitrogen gas at 77 K were performed on each material (Fig. 2 and S1†). Resulting parameters for **1**–**3** are given in Table 1. The specific BET surface area (SA_{BET}) of **1** was determined to be 366 $m^2\ g^{-1}$, with both micropores and mesopores present in the material. After quaternisation of **1** with MeI, the surface area of **2** is lower (166 $m^2\ g^{-1}$) and a further reduction in surface area (to 114 $m^2\ g^{-1}$) is observed upon incorporation of the Rh catalyst in **3**. Pore size analysis of **2** suggests that PSM of **1** results in partial loss of the micropores of the material. The micropore volume ($V_{0.1}$) of **1** is 0.15 $cm^3\ g^{-1}$ but this falls to 0.06 $cm^3\ g^{-1}$ upon quaternisation to yield **2**. Further decrease of micropore volume to 0.04 $cm^3\ g^{-1}$ is observed upon incorporation of the Rh complex to yield **3**. Although there is a further reduction in the total pore volume when the Rh complex is incorporated, the ratio of micropore : total pore volume ($V_{0.1}/V_{tot}$) is unchanged upon transformation of **2** to **3**, suggesting that the Rh complex is situated in the mesopores of the material and which correlates with the loss of hysteresis observed for sample **1** at ~$0.8p/p_0$ on the desorption branch. Finally, the large uptake of gas at high relative pressure ($>0.9p/p_0$) is attributed to the aggregated morphology of the material and shows that even after two PSM steps the morphology of the material remains intact, as further evidenced by transmission electron microscopy (TEM, see below).

The materials are able to form stable dispersions in a wide variety of solvents as previously reported for the PEG-DVB/FN system.[47] This is attributed to the presence of the long solubilising PEG chains which allow the insoluble porous DVB/4VP core network to be dispersed in solution. The stability of an undisturbed dispersion of **1** in $CHCl_3$ was monitored by UV-vis spectroscopy for 72 h (Fig. S2†). Any change in signal intensity is attributed to the material settling out of solution so correlates directly to loss of

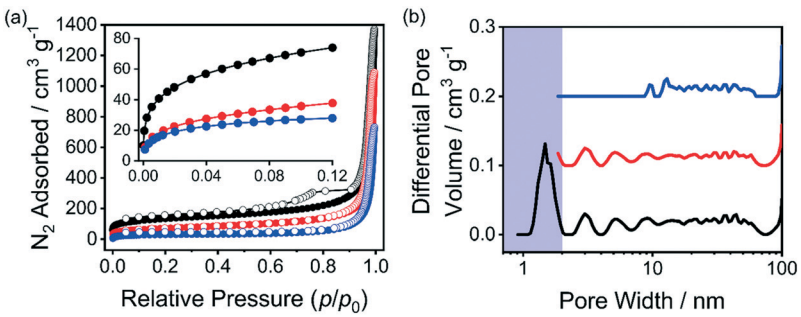

Fig. 2 (a) Nitrogen adsorption (filled) and desorption (open) isotherms at 77 K (offset successively by 25 $cm^3\ g^{-1}$), inset shows the low relative pressure region (with no offset); (b) differential pore size distribution (offset successively by 0.1 $cm^3\ g^{-1}$, micropore region highlighted) of **1** (black), **2** (red) and **3** (blue).

Table 1 Surface areas and pore volumes of polymer nanoparticle samples

Sample	SA_{BET}[a]/$m^2\ g^{-1}$	V_{tot}[b]/$cm^3\ g^{-1}$	$V_{0.1}$[c]/$cm^3\ g^{-1}$	$(V_{0.1}/V_{tot})$
1	366	0.53	0.15	0.28
2	166	0.37	0.06	0.16
3	114	0.25	0.04	0.16

[a] Calculated over the pressure range 0.01–0.15p/p_0. [b] Calculated at 0.99p/p_0. [c] Calculated at 0.1p/p_0.

stability of the dispersion. After 72 h it was found that only ~15% of the sample had settled out of solution and the majority of the polymer was still present as a stable dispersion, indicating suitability for use in a catalytic system as proposed.

The particle size was determined by dynamic light scattering (DLS) and showed that the samples ranged from 190–340 nm in size (Fig. S3†). Our previous studies on related systems have shown that the materials have a complex morphology and are not spherical in shape.[47] DLS assumes a spherical shape and is biased towards larger particles and therefore is unlikely to give an accurate description of the particle size for these samples. Analysis by TEM (Fig. 3b–d) shows this to be the case with DLS likely to be biased towards a longer length of aggregated particles rather than a shorter width. Small-angle X-ray scattering (SAXS) studies were performed on 5% w/w dispersions of samples **1**–**3** in MeOH (Fig. 3a) to gain more detailed insight into the size and morphology of nanoparticles in each sample. The data were successfully fitted using the same two-population model as used previously for PEG-FN/DVB dispersible porous polymers,[47] which suggests the presence of aggregates of smaller primary assemblies, presumably due to both inter- and intra-particle covalent cross-linking (Fig. S4†). Fitting these data indicated that mean diameters for the primary particles (D_1) ranged from 25 nm to 34 nm, with very broad size distributions in each case (standard deviation ≥60%). Remarkably, the mean diameter of the overall aggregates (D_2) remained relatively constant for each sample, with values of 101–104 nm being determined (Table 2). Additionally, the

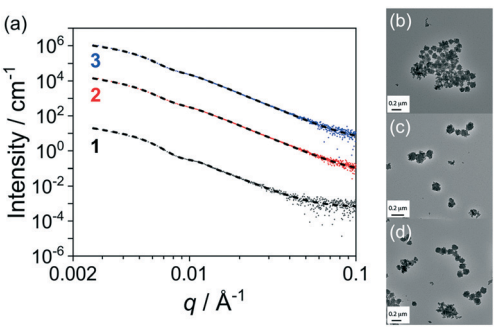

Fig. 3 (a) Small angle X-ray scattering data for sample **1** (black), **2** (red), and **3** (blue) along with two-population fitting (dashed lines). Datasets are offset successively by a factor of 100. TEM images of sample **1** (b), **2** (c), and **3** (d) are also shown.

Table 2 SAXS analysis of samples **1**–**3** where D_1 is the mean diameter of the primary particles and D_2 is the mean diameter of the aggregates

Sample	D_1/nm	D_2/nm
1	25.2 ± 27.1	101.3 ± 15.7
2	31.6 ± 19.8	103.1 ± 20.6
3	34.2 ± 20.3	104.8 ± 19.2

standard deviation in the D_2 values in all cases was significantly lower (≤20%) than that observed for D_1. Importantly, this proposed hierarchical structure is again supported by TEM images (Fig. 3b–d).

Reactivity of supported Rh complex

After soaking a sample of **3** in neat MeI overnight, the IR spectrum of the resulting material displays only one ν(CO) absorption in the terminal metal carbonyl region, at 2058 cm^{-1}, as well as a broad band at ~1700 cm^{-1} (Fig. 4a). This is consistent with formation of a Rh(III) acetyl complex, $[Rh(CO)(COMe)I_3]^-$, resulting from oxidative addition of MeI to *cis*-$[Rh(CO)_2I_2]^-$, followed by spontaneous migratory CO insertion (Scheme 4), analogous to the corresponding reactions observed in solution and in previously investigated polymer-supported systems.[40] Upon exposure of the MeI addition product to CO (1 atm), the IR spectrum gradually changes to resemble that of pristine **3** (Fig. 4a). This could arise either by reversal of the steps described above, with loss of MeI to reform *cis*-$[Rh(CO)_2I_2]^-$, or by coordination of CO to give $[Rh(CO)_2(COMe)I_3]^-$ and subsequent reductive elimination of acetyl iodide. Since no corresponding change in the IR spectrum occurs under N_2, our observations suggest the latter, hence completing the sequence of organometallic steps in the carbonylation cycle (Scheme 1). Although acetyl iodide was not observed directly in this experiment, evidence for formation of organic acetyl species was obtained in experiments at higher temperature and CO pressure (see below).

The stability of dispersions of the polymer-supported complex mean that the organometallic reaction steps can be monitored *in situ* using transmission IR spectroscopy. Fig. 4b shows the terminal ν(CO) region of a series of spectra obtained over the course of the reaction of MeI with **3** dispersed in CH_2Cl_2. The smooth decay of bands due to *cis*-$[Rh(CO)_2I_2]^-$ is apparent, with the terminal ν(CO) band of $[Rh(CO)(COMe)I_3]^-$ appearing close to the high frequency band of the reactant such that these bands are not resolved from each other.

Kinetic data was extracted by monitoring the decay of the low frequency ν(CO) band of *cis*-$[Rh(CO)_2I_2]^-$ at 1987 cm^{-1} over time. Pseudo first-order conditions were ensured by using a large excess of MeI. Fig. 4c shows a typical absorbance *vs.* time plot generated from one of these experiments with the data fitted to a first-order decay curve. It is apparent from this plot that the data are not perfectly fitted by a single exponential decay function. There appear to be two phases during the reaction with an initial faster decay

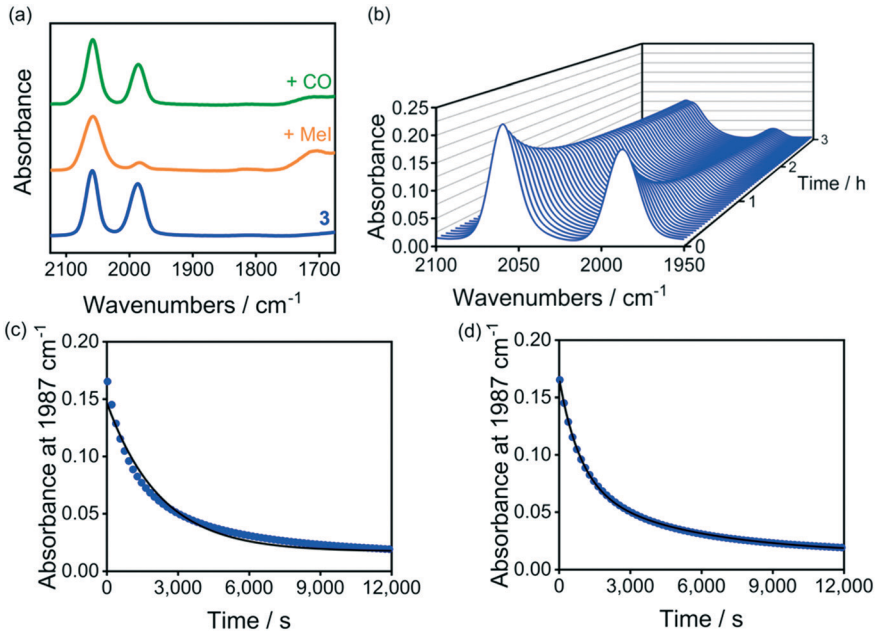

Fig. 4 (a) IR spectra (KBr disc, ν(CO) region) of pristine **3** (blue), after soaking in MeI (orange) and after exposure to CO (green), (b) series of IR spectra (ν(CO) region) during reaction of **3** with 1 M MeI in CH_2Cl_2 (25 °C) and decay of IR absorption at 1987 cm^{-1} during this reaction with (c) single exponential curve fit, and (d) double exponential curve fit.

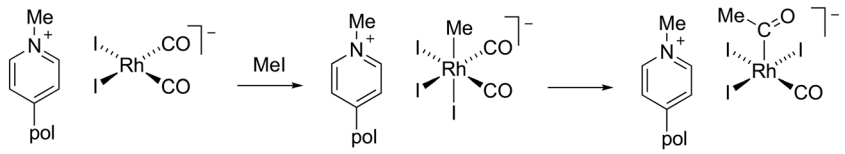

Scheme 4 Reactions of polymer-supported *cis*-$[Rh(CO)_2I_2]^-$ with MeI observed by IR spectroscopy.

followed by a slower downward drift. Empirically it was found that the kinetic data are better described using a double exponential decay, with contributions from two different pseudo first-order rate constants (k_{obs}^1 and k_{obs}^2) as illustrated in Fig. 4d. Analogous experiments were repeated across a range of MeI concentrations (Fig. S4–S8†), giving the pseudo first-order rate constants listed in Table S2.†

Plots of k_{obs}^1 and k_{obs}^2 *vs.* [MeI] (Fig. 5) are approximately linear, with slopes k_2^1 and k_2^2 (Table 3) but have non-zero intercepts. The slow-phase component, k_2^2, is similar to values of the second order rate constant measured for oxidative addition of MeI to $[Rh(CO)_2I_2]^-$ with *N*-methylpyridinium counterions, 4-$RC_5H_4NMe^+$ (R = H, Et, CH_2Ph) in homogeneous solution (Table 3)[51] whereas the fast-phase component, k_2^1 is larger by a factor of ~5. It can be speculated that this kinetic behaviour arises from reactions of complexes in different environments. The similarity of k_2^2 to solution phase data could be attributed to reaction of Rh complex that is more loosely attached to the polymer, perhaps with reversible leaching into the solution phase. If the faster k_2^1 is ascribed to Rh complex within the pores of the dispersed polymer, the question then arises as

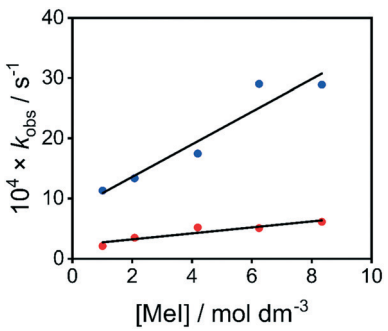

Fig. 5 Plot of k_{obs}^1 (blue, R^2 = 0.92) and k_{obs}^2 (red, R^2 = 0.87) *vs.* MeI concentration for reaction of MeI with **3** in CH_2Cl_2 (25 °C).

Table 3 Second order rate constants for oxidative addition of MeI to $[Rh(CO)_2I_2]^-$ supported on cationic polymer or in solution with various counterions

Cation	$10^5\ k_2/(mol^{-1}\ dm^3\ s^{-1})$
Dispersible polymer (sample **3**)[a]	27 (k_2^1), 5.0 (k_2^2)
Cross-linked polymer film[a]	2.57
Bu_4N^+[a]	2.71
$C_5H_5NMe^+$[b]	4.44
4-$EtC_5H_4NMe^+$[b]	5.75
4-$PhCH_2C_5H_4NMe^+$[b]	4.94

[a] In MeI/CH_2Cl_2, 25 °C. [b] In MeI, 25 °C.

to what causes the higher reactivity in that environment. A five-fold rate enhancement corresponds to a lowering of $\Delta G^{\ddagger}$ of ~4 kJ mol^{-1} so rather subtle effects may be responsible. Activation parameters derived from Eyring plots of variable temperature kinetic data (Table S3 and Fig. S10†) are of a similar magnitude to those reported previously[40] for oxidative addition of MeI to $[Rh(CO)_2I_2]^-$ but the relatively large error margins mean that an enthalpic or entropic origin for the difference between k_2^1 and k_2^2 cannot be discerned.

A number of possible explanations can be considered for the enhanced reactivity of the supported complex: (i) electrostatic interaction of the iodide leaving group with a proximate methylpyridinium moiety of the polymer could stabilise the transition state for the initial S_N2 step in the MeI oxidative addition reaction (Scheme 5a). (ii) A transient highly nucleophilic Rh(I) complex $[Rh(CO)_2I_3]^{2-}$ could form by coordination of an additional iodide ligand (Scheme 5b). This species has been proposed[12] to account for the effect of added iodide salts on the rate of MeI oxidative addition to $[Rh(CO)_2I_2]^-$, although no evidence for direct spectroscopic detection of this dianionic complex has been reported, to our knowledge. (iii) The effective concentration of MeI within the pores of the dispersed polymer may differ from that of the bulk solution. This is unlikely to account for the observed rate enhancement but might make a small (positive or negative) contribution. No rate enhancement was observed for an insoluble cross-linked polymer-supported system studied previously,[40] (Table 3) so the particular structure/morphology or dispersibility of the polymer support in **3** appears to have a significant effect on the oxidative addition rate.

High pressure IR studies

In situ high-pressure IR (HPIR) spectroscopy was used to demonstrate the formation of organic acetyl products by carbonylation of MeOH/MeI using supported catalyst **3** under relatively mild conditions. A dispersion of **3** in MeOH containing 0.8 M MeI was monitored at 120 °C under 10 bar CO pressure. The small effective pathlength of the cell used (see Experimental) meant that IR absorptions due the supported Rh species were not detected in these experiments, but accumulation of organic acetyl products could be observed. IR spectra collected over the course of several hours showed the growth of an absorption at 1736 cm^{-1} due to the ν(C═O) of carbonylation product methyl acetate, with an intensity corresponding to a turnover number (TON) of ~350 after 12 h. Under the conditions used, the ester can be formed by carbonylation of MeI followed by methanolysis of acetyl iodide (Scheme 6a) or by carbonylation of methanol to acetic acid followed by esterification (Scheme 6b). Since the initial MeI : Rh ratio was ~180, the yield of MeOAc cannot be accounted for solely by complete consumption of MeI in the former reaction, so recycling of HI to MeI by reaction with MeOH must occur to complete the full cycle for MeOH carbonylation.

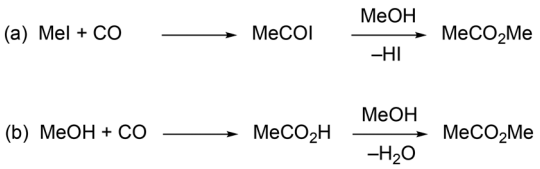

Scheme 6 Carbonylation of (a) methyl iodide or (b) methanol to form methyl acetate.

Growth of the band due to methyl acetate (Fig. 6) was approximately linear for the first 4 h of the reaction, corresponding to an initial turnover frequency (TOF, mol MeOAc/mol Rh per hour) of ~40 h^{-1} but subsequent curvature in the plot shows that the TOF diminishes to ~20 h^{-1} between 9–12 h. The initial rate is approximately double that measured for a homogeneous catalyst ($Bu_4N[Rh(CO)_2I_2]$) under the same conditions (TOF 21 h^{-1}), mirroring the rate enhancement in the oxidative addition kinetic studies (see above). The decrease in reaction rate with time for the supported system could be due to catalyst leaching, deactivation (*e.g.* conversion to inactive $[Rh(CO)_2I_4]^-$) or inefficient recycling of HI to MeI. The polymer material recovered after this experiment by centrifugation was found not to retain carbonylation activity and ICP-MS measurements on the supernatant liquid phase showed that most (>95%) of the rhodium had leached into solution after 24 h. This is probably facilitated in MeOH due to the propensity to form neutral solvent-coordinated Rh complexes (*e.g.* [Rh(CO)I(sol)]) arising from displacement of an iodide ligand, hence breaking the electrostatic attachment to the

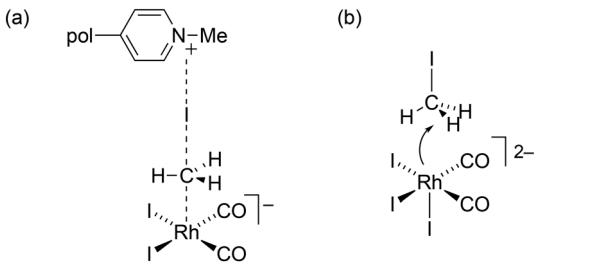

Scheme 5 Potential origins of rate enhancement in polymer (a) electrostatic stabilisation of S_N2 transition state; (b) a highly nucleophilic dianionic Rh(I) species.

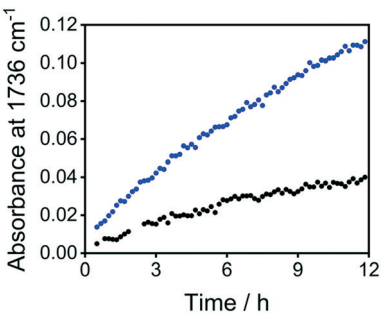

Fig. 6 Plots of absorbance *vs.* time for ν(C═O) of MeOAc during carbonylation experiments using **3** (blue) or $Bu_4N[Rh(CO)_2I_2]$ (grey) (120 °C, 10 bar CO, 0.8 M MeI in MeOH).

polymer support. An experiment using a less polar solvent system (2.5 M MeOH, 0.8 M MeI in $CHCl_3$) gave a slower rate for methyl acetate formation (TOF ~ 11 h^{-1}) but leaching was much reduced (~5% by ICP-MS) and the catalyst recovered by centrifugation retained comparable activity in a subsequent experiment (Fig. S11†).

Conclusions

A dispersible microporous polymer material has been synthesised *via* the co-polymerisation of DVB and 4VP mediated by a PEG-based macro-CTA. Post-synthetic modification of this material was achieved *via N*-methylation of the pyridine moieties with MeI to generate cationic sites on the support, allowing heterogenisation of the anionic carbonylation catalyst, *cis*-$[Rh(CO)_2I_2]^-$, *via* electrostatic interactions. Oxidative addition of MeI to the Rh(I) complex (the rate limiting step in rhodium/iodide catalysed methanol carbonylation) was probed *in situ* using transmission IR spectroscopy. Kinetic experiments showed that the reaction followed a double-exponential decay, possibly indicating different rates for Rh complexes occupying different environments within the microporous polymer or different reactivity for complexes that are more loosely attached to the support. The initial phase of the reaction is faster by a factor of ~5 than for homogeneous analogues with *N*-methylpyridinium counterions. Although the reason for this acceleration is uncertain, it is speculated that transition state stabilisation in an ionic environment or formation of a transient but more nucleophilic Rh(I) complex could be responsible. Formation of methyl acetate by catalytic carbonylation of MeOH/MeI has been demonstrated for catalyst **3** under relatively mild conditions. The carbonylation rate initially surpassed that of a homogeneous analogue but diminished over longer reaction periods with evidence for substantial leaching of Rh catalyst into solution. Leaching (along with carbonylation rate) was reduced in an experiment using $CHCl_3$ solvent.

Dispersible polymer-supported catalysts of the type discussed in this paper present the opportunity to simplify product/catalyst separation and remove catalyst solubility constraints, thereby enhancing process productivity and efficiency. The relatively harsh conditions used for catalytic methanol carbonylation make the development of robust supported catalysts very challenging in that case. However, our results indicate that these support materials can potentially be applied in the design of hybrid homogeneous/heterogeneous catalytic processes that operate under milder conditions with less polar solvents, combining the benefits of efficient mixing in solution with ease of recovery.

Experimental

Synthesis of PEG_{113}-Br

PEG_{113}-Br was prepared in a method similar to that reported previously.[53] Poly(ethylene glycol) monomethyl ether (8 g, 1.6 mmol, 1 eq.) was dissolved in anhydrous toluene (100 mL). Triethylamine (0.32 mL, 2.3 mmol, 1.4 eq.) was added and the solution was cooled to 0 °C. 2-Bromoisobutyryl bromide (0.26 mL, 2.1 mmol, 1.3 eq.) was added dropwise over the course of 1 h before being left to stir overnight at room temperature. The solvent was reduced before being precipitated into cold diethyl ether (200 mL). The crude product was dried under vacuum and dissolved in water before being extracted with CH_2Cl_2. The organic layers were collected, combined and dried over $MgSO_4$ before the solvent was removed under reduced pressure to afford the PEG_{113}-Br product, which was stored at 5 °C (87%), (Anal. found: C, 53.8; H, 9.1. Expected C, 54.0; H, 9.0%).

Synthesis of PEG-based macromolecular chain transfer agent (macro-CTA)

The PEG-based macro-CTA was synthesised in an identical procedure to that previously reported.[47] Dodecane thiol (0.60 mL, 2.5 mmol, 1 eq.) was added to a stirred suspension of K_3PO_4 (0.53 g, 2.5 mmol, 1 eq.) in acetone (50 mL) and stirred for 10 min. Carbon disulfide (0.36 mL, 6 mmol, 2.5 eq.) was added to the suspension and left to stir for a further 10 min. PEG_{113}-Br (10 g, 2 mmol, 0.8 eq.) in acetone (30 mL) was added to the suspension, which was left to stir overnight at room temperature. The solution was concentrated *in vacuo* and the crude product was precipitated by addition of *n*-hexane (100 mL). This was isolated by filtration, dissolved in acetone and the precipitation procedure repeated once more using *n*-hexane and then once using diethyl ether. The sample was dried *in vacuo* at 40 °C for 16 h to afford the RAFT macro-CTA (88%), (Anal. found: C, 54.5; H, 9.1; S, 1.8. Expected: C, 54.5; H, 9.1; S, 1.8%).

Synthesis of 1

The PEG-based macro-CTA (0.26 g, 0.05 mmol, 1 eq.) was added to a 1 : 1 (w/w) mixture of water (228 mL) and ethanol (289 mL) under N_2. DVB (2.13 mL, 15 mmol, 300 eq.) and 4VP (1.65 mL, 15 mmol, 300 eq.) were added to create a 0.83% wt solution. The solution was bubbled with nitrogen gas to remove any oxygen before heating to 70 °C. Polymerisation was initiated through the addition of potassium persulfate (KPS, 2.7 mg, 0.01 mmol, 0.2 eq.) and the mixture was held at 70 °C for 24 h. The product was collected by centrifugation at 4500 rpm for 1 hour before being stirred with diethyl ether to remove any unreacted monomer. Finally, the white solid was isolated through vacuum filtration and dried *in vacuo* at 40 °C for 16 h (0.914 g, 30%), (Anal. found: C, 87.1; H, 7.7; N, 1.7. Expected for $PEG_{113}DVB_{300}4VP_{300}$: C, 84.5; H, 7.4; N, 5.5. Expected for $PEG_{113}DVB_{300}4VP_{60}$: C, 86.8; H, 7.8; N, 1.7%).

Post-synthetic modification of 1 to form 2

A suspension of **1** (596 mg) in a mixture of $CHCl_3$ (60 mL) and MeI (6 mL) was generated by sonication of the mixture for 30 min. This suspension was then stirred at 75 °C under

reflux for 72 h. The resulting yellow suspension was centrifuged at 4500 rpm for 1 h before decanting the supernatant and washing the solid in Et_2O (20 mL × 2). The product was dried under dynamic vacuum at 80 °C for 16 h to give **2** as a yellow powder (564 mg), (Anal. found: C, 76.9; H, 6.9; N, 1.7; I, 10.5. Expected for product with 80% 4VP sites quaternised: C, 77.5; H, 7.1; N, 1.5; I 10.6%).

Post-synthetic modification of 2 to form 3

Dry $CHCl_3$ (40 mL) was added to a mixture of **2** (487 mg) and $[Rh(CO)_2I]_2$ (100 mg, 0.17 mmol) under N_2 gas. The mixture was sonicated for 30 minutes to suspend the nanoparticles and then stirred at room temperature for 16 h. The solvent was removed *in vacuo* and the solid residue was stirred in dry *n*-hexane (50 mL) for 30 min. The solid was collected by filtration and washed with dry *n*-hexane (25 mL × 2). The product was dried under high vacuum for 16 h and then stored at 4 °C under CO. Product **3** was obtained as a brown powder (440 mg) (Anal. found: C, 59.0; H, 5.1; N, 1.9; I, 22.0; Rh, 4.5%). $\nu(C{\equiv}O)/cm^{-1}$ (KBr disc) 2062, 1990.

Kinetic measurements on reaction of 3 with MeI

A dispersion of **3** (~10 mg) in CH_2Cl_2 (3 mL) was generated by sonication of the mixture for 30 min. The required amount of MeI was added to a 2 mL volumetric flask and this was made up to the mark with the suspension of **3** in CH_2Cl_2 and shaken. A sample of the reaction mixture was injected into an IR liquid cell (CaF_2 windows, 0.5 mm path length) fitted with a thermostatted jacket (25 °C). IR spectra in the region 2200–1500 cm^{-1} were recorded at regular intervals, using a spectrum of the appropriate solvent mixture as the background reference. Absorbance *vs.* time data for the frequencies of interest were analysed using Origin software.

Catalytic carbonylation experiments

Reactions were monitored *in situ* by high-pressure IR spectroscopy using a cylindrical internal reflectance (CIR)[54] cell comprising an autoclave (Parr) modified to accommodate a crystalline silicon CIR rod, as described previously.[18,55,56] Spectra were recorded using a Perkin-Elmer Spectrum GX FTIR spectrometer fitted with an MCT detector. The cell was placed directly in the spectrometer sample compartment and aligned to maximise IR energy throughput using a tilt table. A background spectrum was recorded using the appropriate solvent mixture at 120 °C. In a typical procedure, a dispersion of the supported catalyst **3** was generated by addition of dry MeOH (5 mL) to **3** (100 mg) under CO, followed by sonication for 30 min, and stirring for 16 h at room temperature. Separately, MeI (0.5 mL) was added to a 5 mL volumetric flask which was made up to the mark with dry MeOH. This solution and the catalyst suspension were added to the CIR cell and was flushed five times with CO. The cell was then pressurised with CO (10 bar) and heated to 120 °C. IR spectra were recorded at 10 min intervals over the course of 12 h in the region of 2200–1500 cm^{-1}. At the end of the experiment, the solid was recovered by centrifugation. For comparison with a homogeneous system, an experiment was carried out under identical conditions using $[Rh(CO)_2I]_2$ (10 mg, 0.0175 mmol) with Bu_4NI (13 mg, 0.035 mmol) in place of supported catalyst **3**.

Author contributions

S. A. I. and A. M. J. performed the synthesis, characterisation, kinetic and catalytic experiments. M. J. D. performed the SAXS studies. R. D. and A. H. supervised the project. S. A. I., A. M. J., M. J. D., R. D. and A. H. co-wrote the manuscript.

Conflicts of interest

The authors declare no conflicts of interest.

Acknowledgements

The University of Sheffield is thanked for funding PhD studentships (S. A. I. and A. M. J.). Small angle X-ray scattering (SAXS) data were obtained on the I22 beamline at the Diamond Light Source (proposal number SM23501).

References

1 *Applied Homogeneous Catalysis with Organometallic Compounds*, ed. B. Cornils, W. A. Herrmann, M. Beller and R. Paciello, Wiley-VCH, Wenheim, 3rd edn, 2018.
2 A. Behr and P. Neubert, *Applied Homogeneous Catalysis*, Wiley-VCH, Weinheim, 2012.
3 *Catalyst Immobilization: Methods and Applications*, ed. M. Benaglia and A. Puglisi, Wiley-VCH, Weinheim, 2020.
4 K. Shah, in Indian Petrochem Conference, 2014.
5 A. Haynes, in *Adv Catal*, ed. B. C. Gates, H. Knozinger and F. C. Jentoft, 2010, vol. 53, pp. 1–45.
6 R. T. Eby and T. C. Singleton, in *Appl. Ind. Catal.*, 1983, vol. 1, pp. 275–299.
7 P. M. Maitlis, A. Haynes, G. J. Sunley and M. J. Howard, *J. Chem. Soc., Dalton Trans.*, 1996, 2187–2196.
8 D. Forster, *Adv. Organomet. Chem.*, 1979, **17**, 255–267.
9 T. W. Dekleva and D. Forster, *Adv. Catal.*, 1986, **34**, 81–130.
10 F. E. Paulik and J. F. Roth, *Chem. Commun.*, 1968, 1578.
11 D. Forster and T. C. Singleton, *J. Mol. Catal.*, 1982, **17**, 299–314.
12 B. L. Smith, G. P. Torrence, M. A. Murphy and A. Aguiló, *J. Mol. Catal.*, 1987, **39**, 115–136.
13 B. L. Smith, G. P. Torrence, A. Aguilo and J. S. Alder, Hoechst Celanese Corporation, US5001259, 1991.
14 P. Torrence, in *Applied Homogeneous Catalysis with Organometallic Compounds*, ed. B. Cornils and W. A. Herrmann, Wiley-VCH, Weinheim, 2nd edn, 2002, vol. 1, pp. 104–136.
15 J. R. Zoeller, *Catal. Today*, 2009, **140**, 118–126.
16 M. J. Howard, M. D. Jones, M. S. Roberts and S. A. Taylor, *Catal. Today*, 1993, **18**, 325–354.
17 J. H. Jones, *Platinum Met. Rev.*, 2000, **44**, 94–105.

18 A. Haynes, P. M. Maitlis, G. E. Morris, G. J. Sunley, H. Adams, P. W. Badger, C. M. Bowers, D. B. Cook, P. I. P. Elliott, T. Ghaffar, H. Green, T. R. Griffin, M. Payne, J. M. Pearson, M. J. Taylor, P. W. Vickers and R. J. Watt, *J. Am. Chem. Soc.*, 2004, **126**, 2847–2861.
19 Z. Ren, Y. Lyu, X. G. Song and Y. J. Ding, *Appl. Catal., A*, 2020, **595**, 117488.
20 G. A. Flores-Escamilla and J. C. Fierro-Gonzalez, *J. Mol. Catal. A: Chem.*, 2012, **359**, 49–56.
21 N. De Blasio, M. R. Wright, E. Tempesti, C. Mazzocchia and D. J. Cole-Hamilton, *J. Organomet. Chem.*, 1998, **551**, 229–234.
22 L. D. Dingwall, A. F. Lee, J. M. Lynam, K. Wilson, L. Olivi, J. M. S. Deeley, S. Gaemers and G. J. Sunley, *ACS Catal.*, 2012, **2**, 1368–1376.
23 Y. Ni, L. Shi, H. Liu, W. Zhang, Y. Liu, W. Zhu and Z. Liu, *Catal. Sci. Technol.*, 2017, **7**, 4818–4822.
24 T. Yashima, Y. Orikasa, N. Takahashi and N. Hara, *J. Catal.*, 1979, **59**, 53–60.
25 S. Lars, T. Andersson and M. S. Scurrell, *J. Mol. Catal.*, 1983, **18**, 375–380.
26 M. S. Jarrell and B. C. Gates, *J. Catal.*, 1975, **40**, 255–267.
27 N. De Blasio, E. Tempesti, A. Kaddouri, C. Mazzocchia and D. J. Cole-Hamilton, *J. Catal.*, 1998, **176**, 253–259.
28 R. J. Sowden, M. F. Sellin, N. De Blasio and D. J. Cole-Hamilton, *Chem. Commun.*, 1999, 2511–2512.
29 S. Zhang, C. Guo, Q. Qian and G. Yuan, *Catal. Commun.*, 2008, **9**, 853–858.
30 F. Li, B. Chen, Z. Huang, T. Lu, Y. Yuan and G. Yuan, *Green Chem.*, 2013, **15**, 1600–1607.
31 Z. Ren, Y. Lyu, S. Feng, X. Song and Y. Ding, *Mol. Catal.*, 2017, **442**, 83–88.
32 S. Q. Feng, X. S. Lin, X. G. Song, B. B. Mei, J. L. Mu, J. W. Li, Y. Liu, Z. Jiang and Y. J. Ding, *ACS Catal.*, 2021, **11**, 682–690.
33 K. Park, S. Lim, J. H. Baik, H. Kim, K. D. Jung and S. Yoon, *Catal. Sci. Technol.*, 2018, **8**, 2894–2900.
34 D. T. Genna, A. G. Wong-Foy, A. J. Matzger and M. S. Sanford, *J. Am. Chem. Soc.*, 2013, **135**, 10586–10589.
35 X. S. Wang, Y. B. Huang, Z. J. Lin and R. Cao, *Dalton Trans.*, 2014, **43**, 11950–11958.
36 X. Wang, W. Lu, Z.-Y. Gu, Z. Wei and H.-C. Zhou, *Chem. Commun.*, 2016, **52**, 1926–1929.
37 A. Grigoropoulos, A. I. McKay, A. P. Katsoulidis, R. P. Davies, A. Haynes, L. Brammer, J. Xiao, A. S. Weller and M. J. Rosseinsky, *Angew. Chem.*, 2018, **130**, 4622–4627.
38 R. S. Drago, E. D. Nyberg, A. Elamma and A. Zombeck, *Inorg. Chem.*, 1981, **20**, 641–644.
39 N. Yoneda, T. Minami, J. Weiszmann and B. Spehlmann, *Stud. Surf. Sci. Catal.*, 1999, **121**, 93–98.
40 A. Haynes, P. M. Maitlis, R. Quyoum, C. Pulling, H. Adams, S. E. Spey and R. W. Strange, *J. Chem. Soc., Dalton Trans.*, 2002, 2565–2572.
41 P. Kaur, J. T. Hupp and S. T. Nguyen, *ACS Catal.*, 2011, **1**, 819–835.
42 M. Rose, *ChemCatChem*, 2014, **6**, 1166–1182.
43 Q. Sun, Z. Dai, X. Meng and F. S. Xiao, *Chem. Soc. Rev.*, 2015, **44**, 6018–6034.
44 S. Fischer, J. Schmidt, P. Strauch and A. Thomas, *Angew. Chem., Int. Ed.*, 2013, **52**, 12174–12178.
45 L. Li, C. Cui, W. Su, Y. Wang and R. Wang, *Nano Res.*, 2016, **9**, 779–786.
46 W. Zhao, F. Zhang, L. Yang, S. Bi, D. Wu, Y. Yao, M. Wagner, R. Graf, M. R. Hansen, X. Zhuang and X. Feng, *J. Mater. Chem. A*, 2016, **4**, 15162–15168.
47 A. M. James, M. J. Derry, J. S. Train and R. Dawson, *Polym. Chem.*, 2019, **10**, 3879–3886.
48 C. T. J. Ferguson, N. Huber, T. Kuckhoff, K. A. I. Zhang and K. Landfester, *J. Mater. Chem. A*, 2020, **8**, 1072–1076.
49 A. M. James and R. Dawson, *Macromol. Rapid Commun.*, 2020, **2000176**, 1–5.
50 F. A. L. Anet and I. Yavari, *J. Org. Chem.*, 1976, **41**, 3589–3591.
51 A. Fulford, C. E. Hickey and P. M. Maitlis, *J. Organomet. Chem.*, 1990, **398**, 311–323.
52 A. Haynes, B. E. Mann, G. E. Morris and P. M. Maitlis, *J. Am. Chem. Soc.*, 1993, **115**, 4093–4100.
53 J. Chen, M. Liu, H. Gong, Y. Huang and C. Chen, *J. Phys. Chem. B*, 2011, **115**, 14947–14955.
54 W. R. Moser, J. E. Cnossen, A. W. Wang and S. A. Krouse, *J. Catal.*, 1985, **95**, 21–32.
55 J. M. Birbeck, A. Haynes, H. Adams, L. Damoense and S. Otto, *ACS Catal.*, 2012, **2**, 2512–2523.
56 S. E. Repper, A. Haynes, E. J. Ditzel and G. J. Sunley, *Dalton Trans.*, 2017, **46**, 2821–2828.